Hindawi
International Journal of Photoenergy
Volume 2018, Article ID 4030214, 14 pages
https://doi.org/10.1155/2018/4030214

Research Article

A Five-Level H-Bridge STATCOM for an Off-Grid PV Solar Farm under Two Controllers PI and PI$^{\lambda}$-MPC Hybrid

Onur Ozdal Mengi

Department of Energy Systems Engineering, Engineering Faculty, Giresun University, 28100 Giresun, Turkey

Correspondence should be addressed to Onur Ozdal Mengi; onurmengi@yahoo.com

Received 6 December 2017; Revised 1 February 2018; Accepted 20 February 2018; Published 4 April 2018

Academic Editor: Mahmoud M. El-Nahass

Investigations were presented in order to eliminate the reactive power on microgrid loads fed by an off-grid and mid-power photovoltaic solar energy system (PVSES) with a static synchronous compensator (STATCOM) device. The electric network is specifically characterized by P-Q loads, ambient temperature, and widely variable solar radiation levels. Two main innovations are developed. Firstly, the STATCOM apparatus is a 5-level H-bridge inverter with capacitances as load and must totally compensates the reactive power in the network load. Secondly, this compensation is controlled by a set of fractional PI (PI$^{\lambda}$) and model predictive control (MPC) hybrid. The efficiencies of these controllers were compared with classical PI controllers. Large simulations, without and with reactive power compensation, in steady and transient states, are carried out to underline the merits of the presented works, by performing in the MATLAB-Simulink environment.

1. Introduction

The sun warms our planet with the resulting energy released from nuclear explosions taken place within itself and makes our planet a place to live for people, animals, and plants. The sun, which is our source of life along with the rapid progress of technology, now also serves as an energy source. Photovoltaic solar cells are systems that convert solar energy from sunlight into electricity and thus produce electricity. Solar cells come together to form panels, and the panels come together to form PVSESs [1]. The solar panels generate DC voltage at the output. The DC voltage and power obtained from the solar panels are used to feed either DC loads or AC loads by converting it to AC voltage via an inverter. Various solar cell production techniques and materials have been developed. There are many solar panels made of numerous materials such as amorphous silicon, copper indium gallium selenide, and cadmium telluride [2]. The costs and efficiencies of these panels are quite different. Nowadays, solar cells yielding 35% of efficiency have been produced [3].

Large scale applications have become more economical with the development of solar panel production techniques, the increase in production, and also the increase in panel power values and yields [4]. As a result of these, large power plants have been begun to build from large scale photovoltaic solar panels [5]. These power plants are on-grid or off-grid [6]. In off-grid PVSESs, compensation must be applied to the system for reducing harmonics caused by the loads having reactive power and preventing injecting of the reactive power from the source [7, 8]. There are many different compensation techniques. Among them, voltage source converter- (VSC-) based compensators are the Static VAR Compensator (SVC), STATCOM, Thyristor Controlled Series Compensator (TCSC), Static Synchronous Series Compensator (SSSC), and Unified Power Flow Controller (UPFC) [9]. STATCOMs are one of the dynamic systems capable of doing this [10, 11]. STATCOMs are able to do compensation by appropriately switching the reactive power generated by capacitors. In general, IGBT, thyristor, and transistor are used for switching. These components are switched by techniques such as Pulse Width Modulation (PWM) and Sinusoidal Pulse Width Modulation (SPWM) [12]. There are different topologies in the inner structure of the STATCOM. These systems, which are usually multilevel inverters, are switched by appropriate control techniques. Current source,

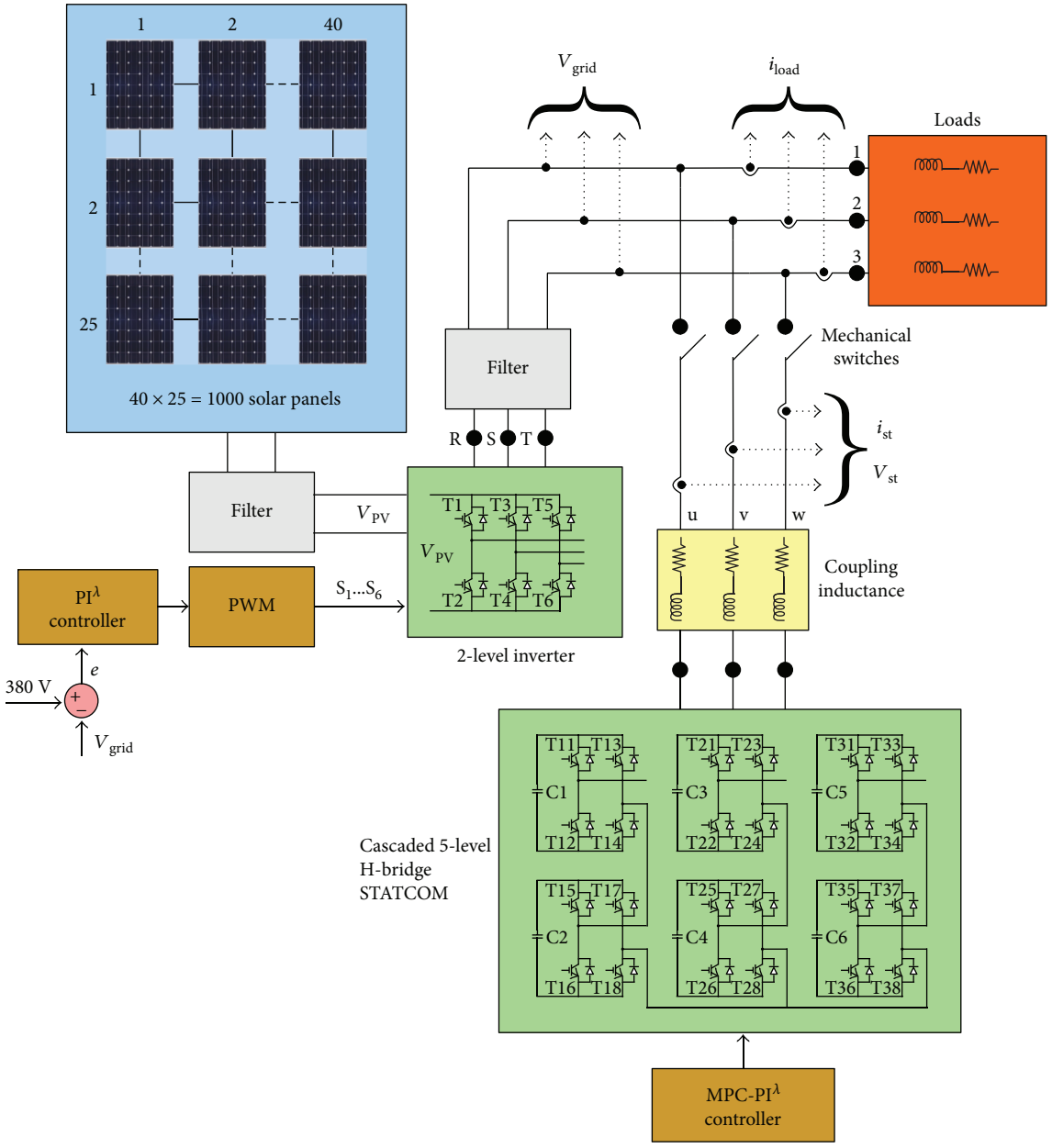

Figure 1: PVSES with a STATCOM device.

voltage source, impedance source, quasi impedance source inverters, and multilevel inverters are commonly used [13]. These inverters are controlled by using classical and advanced control methods such as a PID controller [14], fuzzy logic controllers [15], fractional PID [16], artificial neural networks [17], vector control methods [18], model predictive control [19], and genetic algorithms [20].

The innovation carried out by this study is the implementation of a five-level H inverter for the STATCOM converter (including 24 IGBT-s transistors). In addition, this device allows eliminating the load reactive powers, to regulate the network voltage by increasing its efficiency and reducing harmonics contained in the electric network. The plant is fed by an off-grid photovoltaic solar power generation system, and the STATCOM converter is controlled by PI$^{\lambda}$ and MPC. The efficiency of the obtained advanced control structure was compared using classical PI controllers. The voltages on loads were tried to keep constant at a value of 380 V/50 Hz with a classical 2-level three-phase voltage. It has been tried to create challenging conditions by continuously changing the loads, ambient temperature, and the solar irradiation level. In this environment, the performances of the controllers were tested and the contribution of the advanced control techniques was addressed by comparing the results obtained. All of the simulation was performed in the MATLAB/Simulink environment.

This paper is organized in four sections. Section 1 contains the introduction. The STATCOM device and controllers

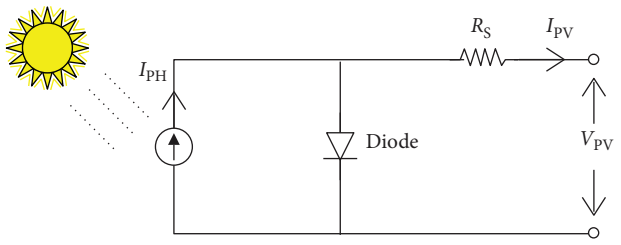

Figure 2: Equivalent circuit model of a PV solar cell.

are described in Section 2. Section 3 presents simulation results. The last section gives some remarks and conclusion.

2. Materials and Methods

The overall scheme of the proposed PVSES and STATCOM system was given in Figure 1. The system consisted of solar panels, filters, inverters, loads, measuring components, and a STATCOM device.

The solar panels contained 25 parallel branches and 40 panels in each branch. The PV solar panels' output filter has a 6.5 μF capacitor. The voltage obtained from these panels was converted to 380 V/50 Hz AC voltage through a 2-level inverter before passing from a filter. The two-level inverter output filter consisted of a 22 μF capacitor and 2 mH inductance. This inverter is switched using PI controllers, and carrier frequency is 2 kHz.

The STATCOM device consisted of 5-level H-bridge IGBTs, capacitors, and a control unit. These controllers here were used to control the capacitor voltages and IGBTs. Capacitor voltage was controlled by PI$^{\lambda}$, and IGBTs were controlled by MPC. The STATCOM device was connected to point of common coupling (PCC) via a coupling inductance. Different resistive and motor loads were used as loads.

2.1. PV System. Photovoltaic solar cells are semiconductor components that turn solar light to electrical energy. There are different equivalent circuit models. The equivalent circuit model with one diode of a solar panel is seen in Figure 2 [21, 22].

The output voltage of the PV cell is as in (1) [23].

$$V_{PV} = \frac{N}{\lambda}\ln\left(\frac{I_{SC} - I_{PV} + MI_0}{MI_0}\right) - \frac{N}{M}R_s I_{PV}. \quad (1)$$

Descriptions of the variables used here are seen in Table 1.

2.2. STATCOM Device. A STATCOM is a parallel-connected static synchronous compensator. The STATCOM is a FACTS device that continuously supplies reactive power to or injects reactive power from the system that it is connected. STATCOM has important features such as having a fast response time and fewer space requirements and showing very good dynamic characteristic under different operating conditions [24].

Table 1: The descriptions for the PV cell.

Expression	Definition	Unit
V_{PV}	Cell output voltage	V
I_{PH}	Photocurrent, function of irradiation level, and junction of temperature	A
I_{PV}	Cell output current	A
I_{SC}	Cell short-circuit current	A
I_0	Reverse saturation current	A
R_S	Series resistance of the cell	Ω
N	Series cells per string	
λ	Constant coefficient and depends upon the cell material	
M	Parallel strings	

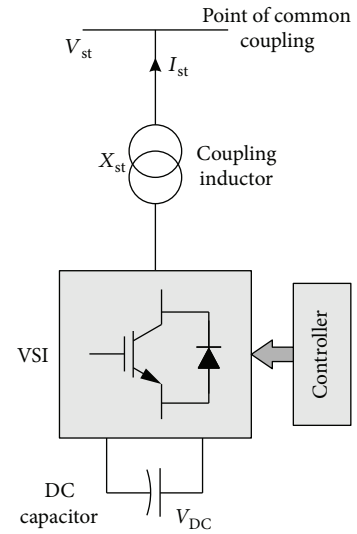

Figure 3: Basic structure of the STATCOM device.

The active and reactive power exchanges between the STATCOM and the system are given by (2).

$$P_{st} = \frac{V_{st}V_s}{X_{st}}\sin\delta,$$
$$Q_{st} = \frac{V_s}{X_{st}}(V_s - V_{st}\cos\delta). \quad (2)$$

V_s is system voltage, V_{st} is STATCOM voltage, and δ is the phase angle between V_{st} and V_s. X_{st} is reactance between the STATCOM and the system. L_{st} is an inductive part of the X_{st}.

The basic structure of the STATCOM device is shown in Figure 3.

The values of the passive elements of the STATCOM are calculated in (3) and (4).

$$C_{dc} = \frac{\sqrt{2}\cdot I_{RMS}}{\omega\cdot\Delta V_{pp}}\left[1 - \sin\left(\arccos\left(\frac{M_{max}\pi}{4}\right)\right)\right]. \quad (3)$$

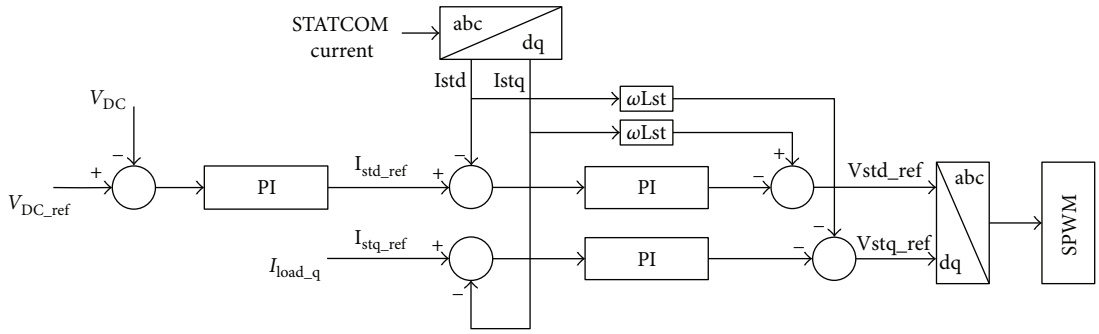

Figure 4: General block diagram of an indirect current controller.

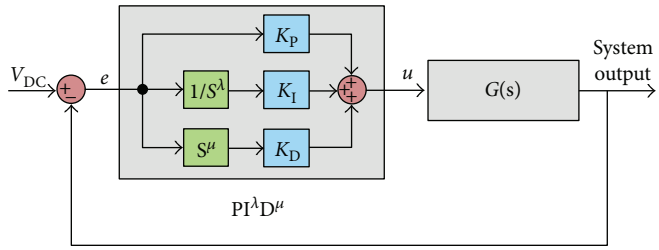

Figure 5: General block diagram of a $PI^{\lambda}D^{\mu}$ controller.

I_{RMS} is the RMS value of the system current, ΔV_{pp} is peak to peak variation of the three-phase system voltage, M_{max} is the maximum value of the modulation index.

$$\frac{V_{DC}}{8f_s(n_{Level}-1)\Delta I_r} \le L \le \frac{V_{st}-V_s}{I_{load\_f}\omega I_{st}}. \quad (4)$$

V_{DC} is DC voltage of the STATCOM, f_s is PWM frequency, ΔI_r is current ripple, V_{st} is VSI voltage, V_s is system voltage, I_{load_f} is the fundamental harmonic component of the load current, ω is angular velocity, I_{st} is the RMS value of VSI output current, and n_{Level} is the number of the inverter level [25, 26].

In this study, the five-level H-bridge STATCOM device is used. The reason of this, 3-level inverters give lower quality results and 7-level inverters have much more complicated results because of using too much IGBTs.

2.3. STATCOM Device Control Structure with a Classical PI Controller. Various structures for the STATCOM device control are used in literature. One of them is the indirect current control method [26]. In this method, generally, classical PI controllers are used. This control structure is shown in Figure 4.

In Figure 4, I_{load_q} is defined as the reactive component of load current.

2.4. Fractional PID Controller ($PI^{\lambda}D^{\mu}$). $PI^{\lambda}D^{\mu}$ controllers are advanced controllers that can give better results than classical PI controllers. They are widely used because they are able to adjust more precisely than PID controllers. The best knowns are the descriptions of Caputo, Grunwald-Letkinov, and Reimann-Liouville [27, 28]. The $PI^{\lambda}D^{\mu}$ controller general block diagram is shown in Figure 5.

System output, $C(s)$, is as seen in (5).

$$C(s) = \frac{U(s)}{E(s)} = K_P + \frac{K_I}{s^{\lambda}} + K_D s^{\mu}. \quad (5)$$

Here, λ and $\mu \ge 0$. λ is the order of integration, and μ is the order of the differentiator. K_P, K_I, and K_D are the PID controller gains. $U(s)$ and $E(s)$ are the control and error signals, respectively. In this study, $PI^{\lambda}D^{\mu}$ controller software was performed by FOMCON toolbox [29].

2.5. Model Predictive Controller (MPC). MPC is a control technique designed on the basis of the prediction of behavior of the systems in the next step. It is aimed at estimating the next possible switching states and providing the selection of switching that minimizes the error over the existing states. To achieve this, a correct model of the system has to be revealed. At each sampling time, the control of a particular topology defines a cost function that is minimized as an optimization problem. The general application of MPC in the STATCOM device is as shown in Figure 6.

MPC generally consists of two groups: finite control set MPC and continuous control set MPC. They are divided into two groups among themselves. Finite control set MPC is divided into optimal switching vector MPC

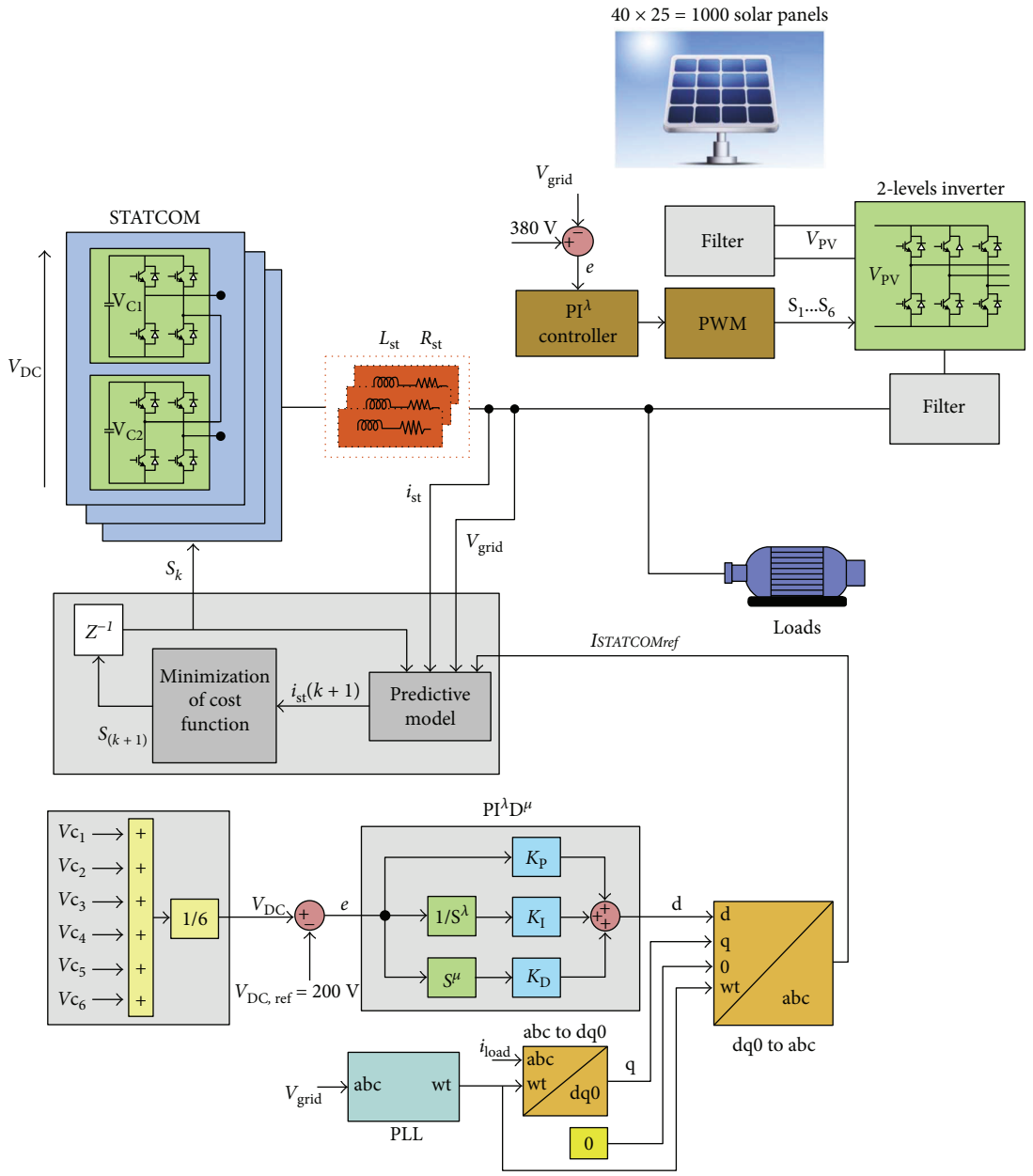

Figure 6: Block diagram of MPC for the STATCOM device.

and optimal switching sequence MPC, and continuous control set MPC is divided into generalized predictive control and explicit MPC. In the simulation, an optimal switching vector MPC technique was used because it does not need a modulator and fixed switching frequency, it is intuitive, and it can perform online optimization [30]. The predictive control technique can be used easily in multilevel STATCOM applications.

For multilevel STATCOMs, the AC side equality is as in (6).

$$V_s^{abc} = L_{st} \frac{d}{dt} i_{st}^{abc} + R_{st} i_{st}^{abc} + V_{st}^{abc}. \quad (6)$$

Table 2: Photovoltaic solar panel parameters.

Value	Unit
Open-circuit voltage	36.3 V
Short-circuit current	7.84 A
Maximum power	213.15 W
Voltage at maximum power point	29 V
Current at maximum power point	7.35 A
Temperature coefficient of short-circuit current	0.102%/deg.C
Temperature coefficient of open-circuit voltage	−0.36%/deg.C
Serial resistance	0.39 ohm
Diode saturation current	2.92e-10 A
Diode ideality factor	0.98

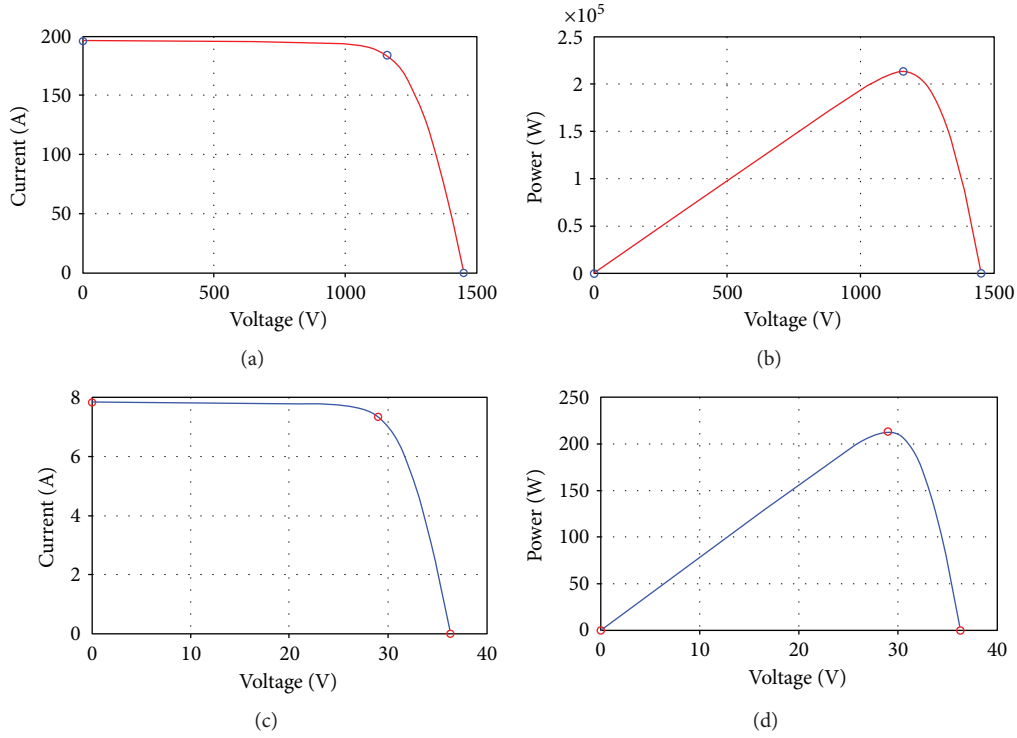

Figure 7: (a) Total PVSES output V-I diagram, (b) total PVSES output V-P diagram, (c) a photovoltaic solar panel V-I diagram, (d) a photovoltaic solar panel V-P diagram.

If i_{st}^{abc} is extracted and discretized from (6), its next value can be computed from (7).

$$i_{st}^{abc}(k+1) = \left(1 - T_s \frac{R_{st}}{L_{st}}\right) i_{st}^{abc}(k) + \frac{T_s}{L_{st}} \left\{ V_s^{abc}(k) - V_{st}^{abc}(k) \right\}. \tag{7}$$

Here, T_s is the sampling time. k expresses the current states of the variables. $k+1$ is used to predict the future behavior of the system. R_{st} is a coupling resistor, L_{st} is a coupling inductance, i_{st}^{abc} is 3-phase STATCOM current, V_s^{abc} is 3-phase grid voltage, and V_{st}^{abc} is 3-phase STATCOM voltage.

A cost function should then be used. This cost function should evaluate the all possible switching combinations, choose the option minimizing cost function, and apply it in the next step. The cost function used to minimize the current error is as in (8) [31].

$$g = \left| i_{st}^{abc,ref}(k+1) - i_{st}^{abc}(k+1) \right|. \tag{8}$$

3. Results and Discussion

Firstly, the installed system was run without the STATCOM device. What happened in this case was investigated. Then, the STATCOM device with a PI controller and finally the PI$^{\lambda}$-MPC hybrid controller were used, and their results were shown. In all the simulations, the total power of the photovoltaic solar panels and the system used in PVSES were kept same.

3.1. Data of PV Panels. The solar panels are commercially available and have the characteristics as defined in Table 2. The passive elements of the STATCOM device consist of 4700 μF capacitors and of coupling inductance with 56 mΩ and 12 mH [32]. In Figure 7 are shown the exploitation curves of each panel and the set of panels (40 in series and 25 in parallel).

Figure 7 and Table 2 define the data used in commercial PV panels.

Also, in all the simulations, the ambient temperature level and solar irradiation level were changed according to Figure 8.

3.2. Simulation Results and Discussion. Here, the PV filter has a 6.5 μF capacitor. The voltage obtained from these panels was converted to RMS phase-to-phase voltage 380 V under 50 Hz AC voltage through a 2-level inverter before passing from a filter. This filter consists of a 22 μF capacitor and 2 mH inductance. The system sampling time is 5 μs. PV panel output voltage changes between 1200 V and 1350 V, and output current changes up to 150A.

The installed system was tested using variable loads, according to Table 3 for their connection and disconnection times.

In addition, during the time simulation (between 0 and 1 s), ambient solar irradiation and temperature change as shown in Figure 8.

3.2.1. Case 1: Installation without the STATCOM Device (Mechanical Switch Open). The two-level inverter is switched using PI controllers, and carrier frequency is 2 kHz, involving

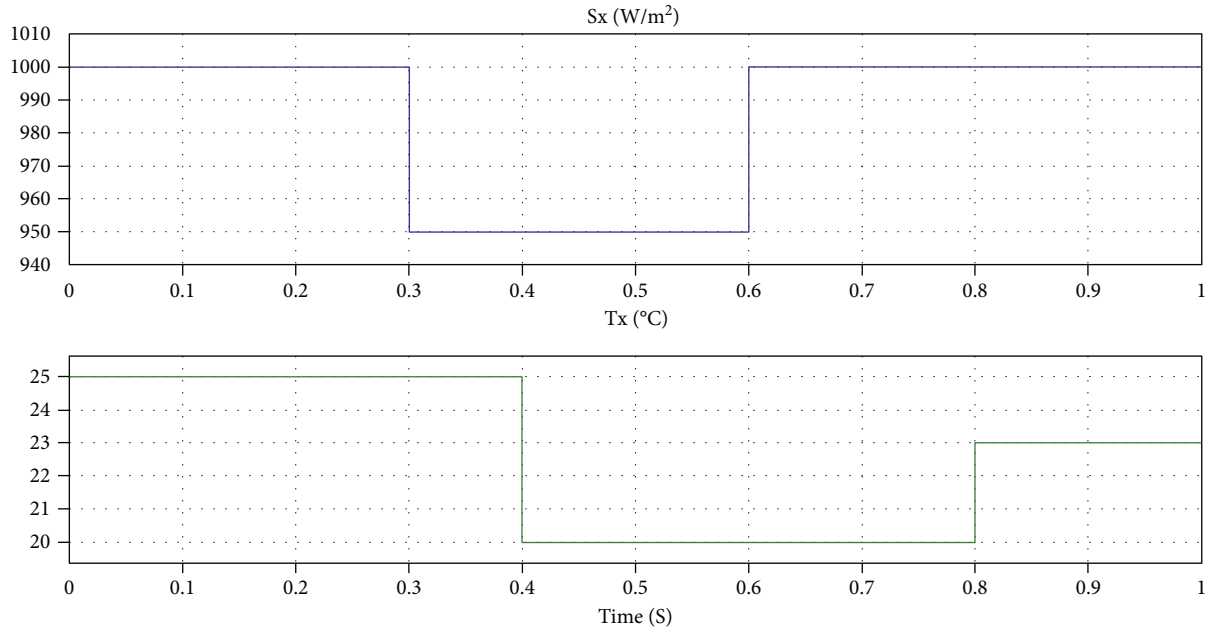

Figure 8: Ambient solar irradiation level and temperature changes.

Table 3: Loads used in the system and times that they entered the circuit.

Load type	Value	Commutation times (s)
R	+50 kW	t1 = 0: connection
RL	+10 kW/+10 kVAr	t2 = 0.3: connection
RL	−10 kW/−10kVAr	t3 = 0.45: disconnection
R	+5 kW	t4 = 0.6: connection
L	+5 kVAr	t5 = 0.8: connection

a pulse width modulation principle. In the absence of the STATCOM device, the compensation of reactive power cannot not be performed. The graphs obtained in this case are shown in Figure 9.

Figure 9 shows that the reactive power taken by the load cannot be compensated when there is no STATCOM device in the system. The same reactive power was present on the load and the grid side.

In Figure 9, change in the voltage amplitude on the loads is shown. PI controllers kept the load voltage constant at 380 V. Here, 2-level IGBTs inverters were used. PI controllers that set the load voltage were also set to $K_P = 0.5$, $K_I = 100$. These values were found by different simulations work on this system. The controller could hold magnificently the RMS phase-to-phase load voltage constant at 380 V. The change was around ±5 V.

As shown in this figure, the dispersion of RMS phase-to-phase voltage is very negligible: around 1 V/380 V and after sudden changes of load, we notice: for $\Delta_2 = -5$ V; for $\Delta_3 = +5.8$ V; $\Delta_5 = -1$ V. And the disturbance duration are lesser 25 ms.

3.2.2. Case 2: STATCOM with a PI Controller. The results obtained when an indirect current control method with PI controllers were used to control both the V_{DC} voltage and the switching signals are shown in Figures 10 and 11. The ambient conditions and also the constant change in loads forced the system. PI controllers used in an indirect current control method were set to $K_P = 5$ and $K_I = 40$. For PI controllers that adjust the load voltage, $K_P = 0.5$ and $K_I = 100$ were also taken. This value is the same as the values used in the case without the STATCOM device.

Figure 10 shows the switching states belonging to a phase when the STATCOM with a PI controller is enabled. The first two graphs show the switchings of IGBTs on the first H-bridge (triggers of T11 and T12) and the other two on the second H-bridge (triggers of T15 and T16). While two IGBTs on each bridge were switched, the opposite way of the switchings was sent to the other two.

Figure 12 shows the efficiency of the STATCOM device. The reactive power compensation was performed successfully. The reactive power take from the grid was zero.

Also, Figure 12 shows change in the tension on loads. Although PI controllers had a high overshoot value, they kept the load voltage at 380 quite well. The PI controller constants were $K_P = 0.5$ and $K_I = 100$. These values are deduced by trial and error.

As shown in this figure, overshoot is too bad. This value reach 465 V. So, ΔV_O is +85 V. Nevertheless, ΔV_2 and ΔV_3 are negligible. Between t_2 and t_3, the reactive power residue is approximately +300 VAr.

In Figure 13, each DC capacitor voltage V_{DC} in the STATCOM device were kept at 200 V and the capacitor voltage on H-bridge converter is perfectly balanced. This underlines that the more the controllers efficiently operate, the compensation action is more performing.

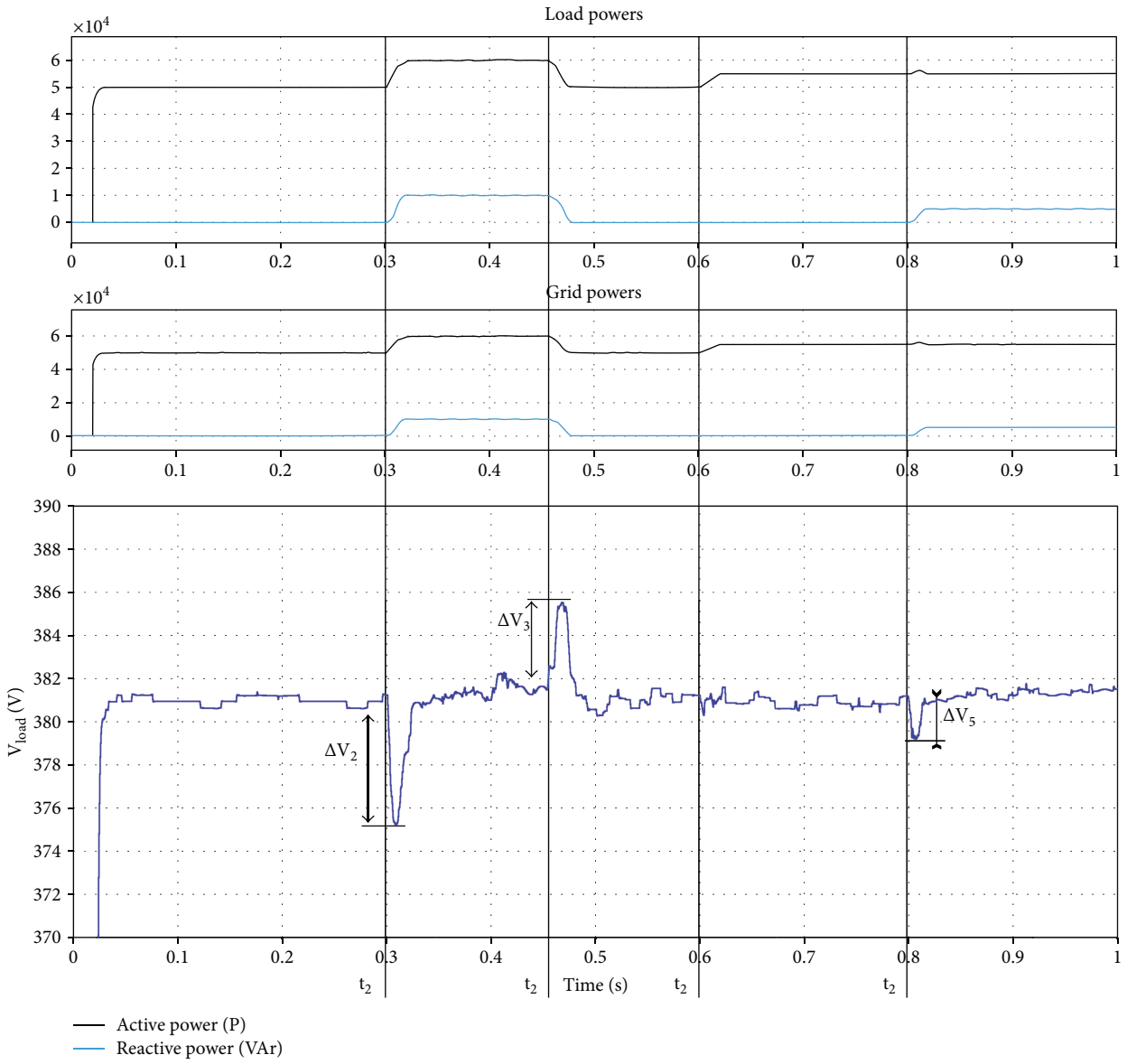

Figure 9: Active, reactive power, and load voltage states on the system.

Figure 11 shows FFT analysis of the PVSES system output voltage and current. For the phase-to-neutral voltage, the shape is perfectly sinusoidal and the module gap difference is lesser than 1%.

3.2.3. Case 3: STATCOM with a PI$^{\lambda}$-MPC Hybrid Controller. The results obtained in using PI$^{\lambda}$-MPC hybrid controllers to control both V_{DC} voltage and switching signals are shown in Figures 14 and 15. Here, V_{DC} voltage was controlled by PI$^{\lambda}$ and the switching signals in a 24 IGBTs 5-level STATCOM device were controlled by MPC. Both ambient conditions and loads are constantly changing.

The switching states belonging to a phase when the STATCOM device with a PI$^{\lambda}$-MPC hybrid controller is enabled are shown in Figure 14 (the first two graphs: triggers of T_{11} and T_{12}, and the other two: triggers of T_{15} and T_{16}). The switching signals are different than in the case using PI controllers. These signals took randomly in the time scale.

Figure 16 shows the efficiency of the STATCOM device with a PI$^{\lambda}$-MPC hybrid controller. The reactive power compensation was performed successfully. The reactive power taken from the grid was zero. The fluctuation was less than in the case using a PI controller.

This figure shows change in the voltage on loads. Overshoot and settling time values were better than PI controllers. For PI$^{\lambda}$ controllers that adjust the load voltage, $K_P = 0.5$, $K_I = 100$, and $\lambda = 1.2$ were taken. As shown in this figure, overshoot is very low. This value reach 384 V. So, ΔV_O is +4 V. But, sudden load changes like at ΔV_2, ΔV_3, and ΔV_5 are important. Despite the change in voltage on the load, the reactive power is well compensated. At this time,

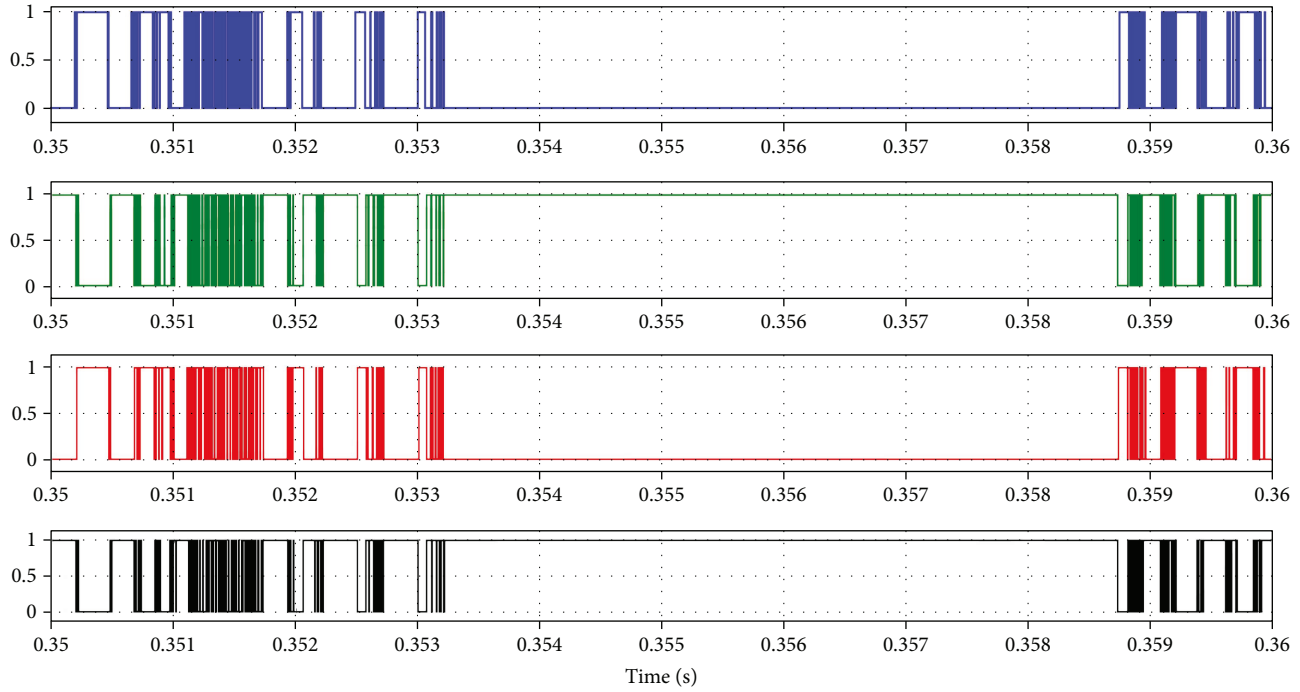

Figure 10: Switchings belonging to a phase when the STATCOM device with a PI controller is enabled.

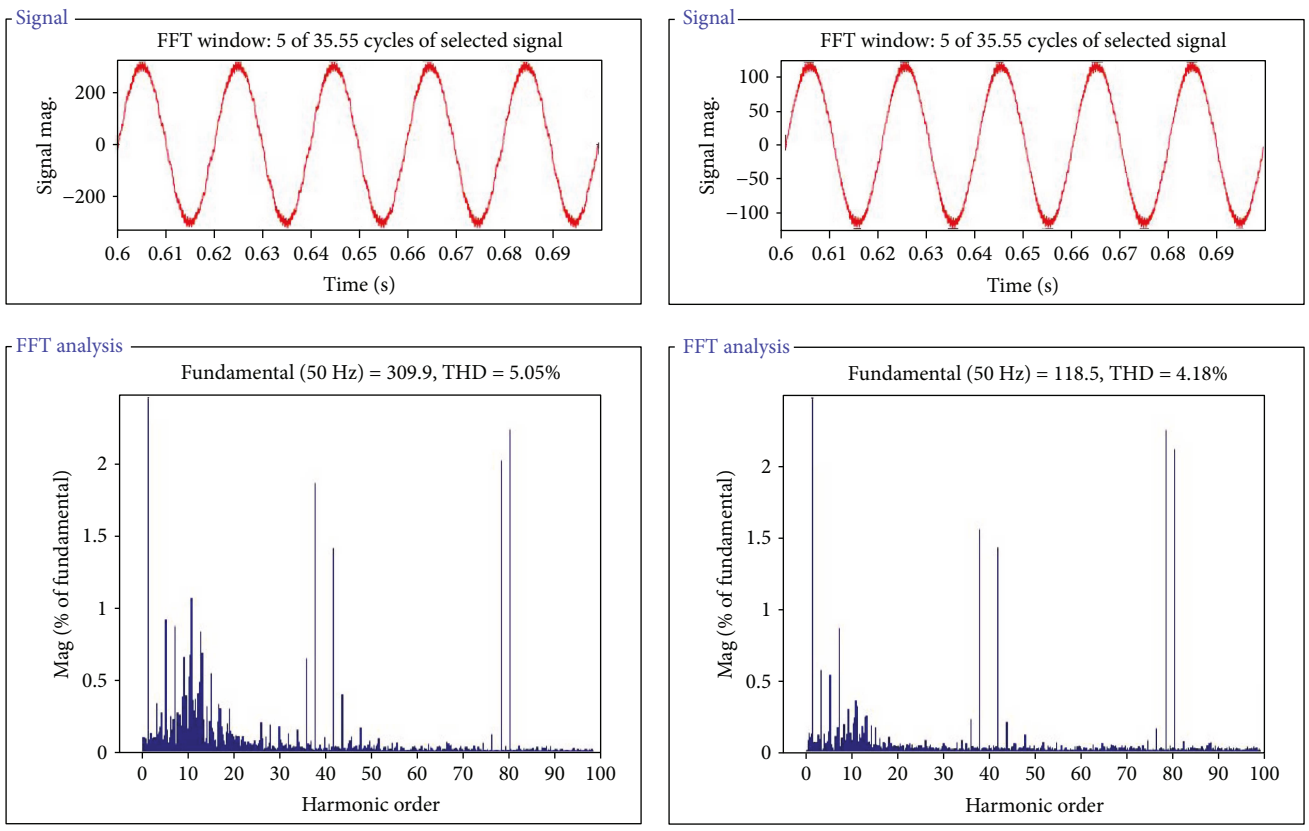

(a) Voltage FFT analysis

(b) Current FFT analysis

Figure 11: FFT analysis of phase to neutral voltage and line current on the electric network of the system.

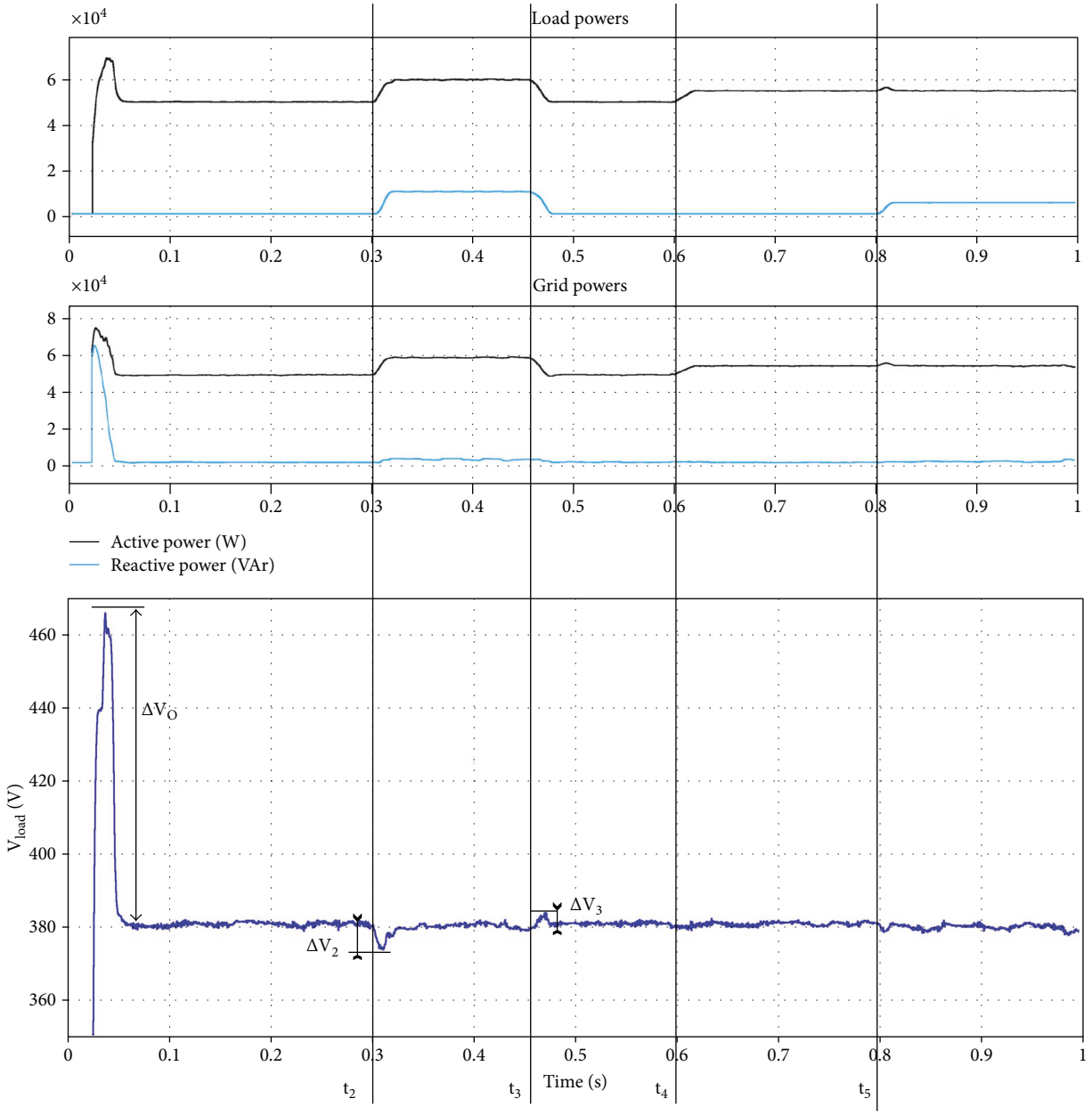

Figure 12: Reactive power compensation when the STATCOM device with a PI controller is enabled and voltage change on loads.

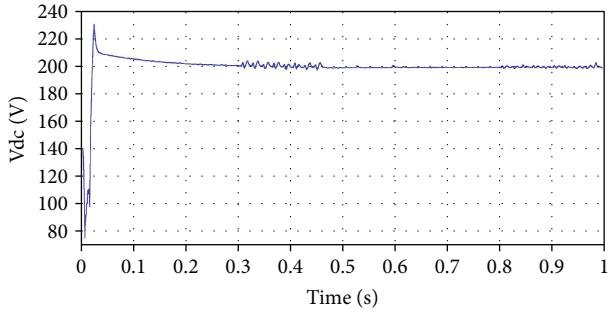

Figure 13: Capacitor voltage control in the STATCOM device with a PI-controller.

reactive power on the system is approximately +50 VAr. This is a too low value.

Figure 17 shows that the capacitor voltages in the STATCOM device are kept at 200 V. Both settling time and overshoot values were much better than the case using a PI controller. Also, the fluctuations in the load changes were less. Here, the PI^{λ}-type controller was used. In PI^{λ} controllers used both in the setting of voltage on load and in the controlling of V_{DC} voltage in the STATCOM, controller parameters are $K_P = 5$, $K_I = 40$, ve $\lambda = 1.2$ were taken.

Figure 15 underlines the good results shown in Figure 11 (the same values about the modulus of phase-to-neutral and its THD).

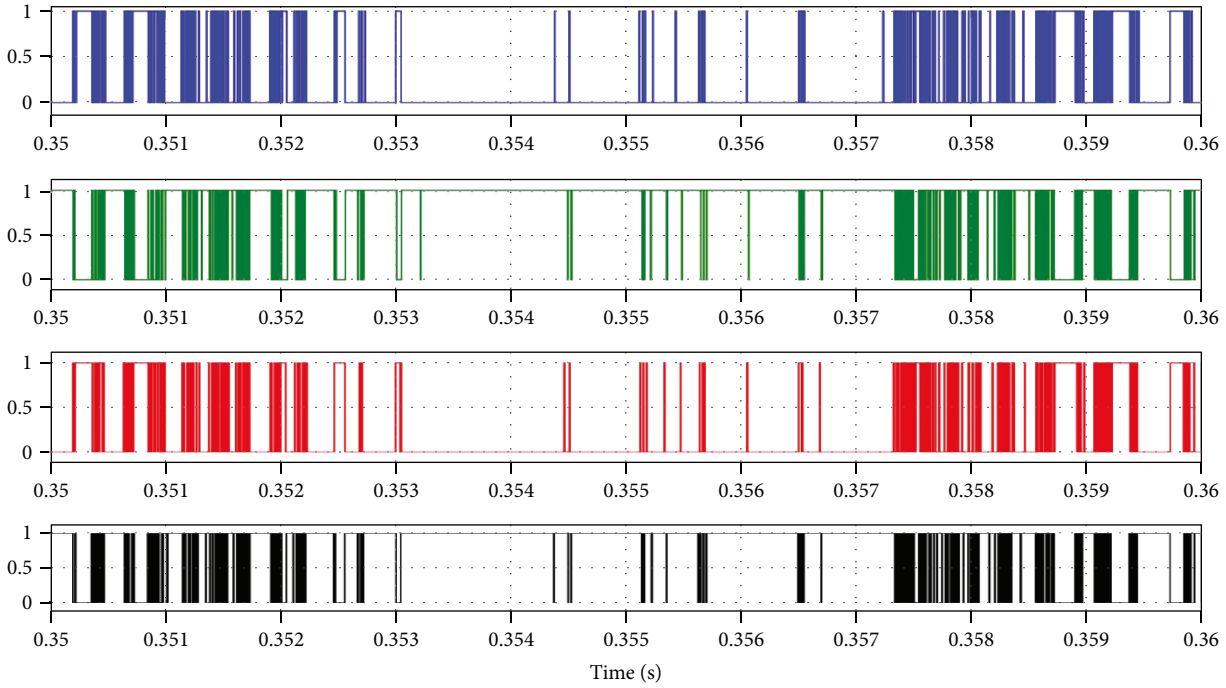

Figure 14: Switchings belonging to a phase when the PI$^{\lambda}$-MPC hybrid controller is enabled.

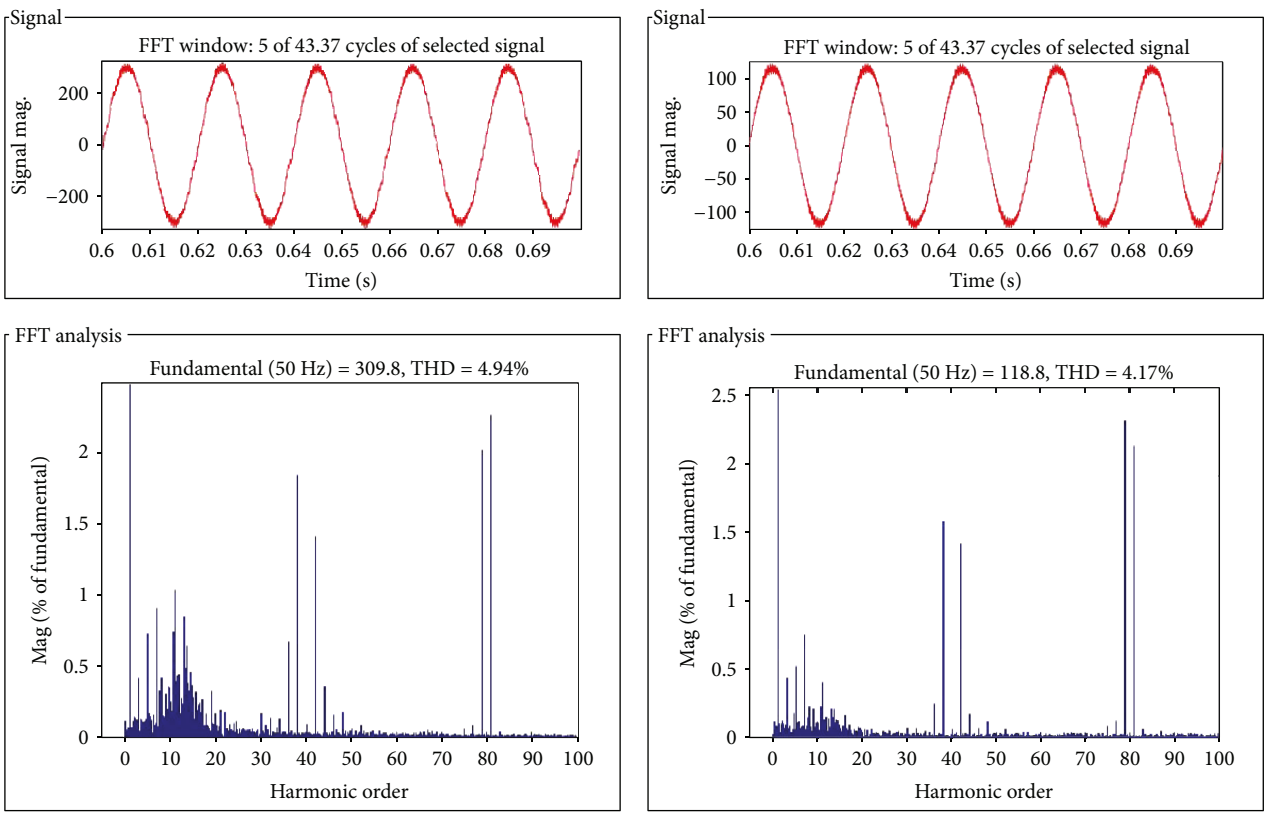

(a) Voltage FFT analysis

(b) Current FFT analysis

Figure 15: FFT analysis of a PVSES system.

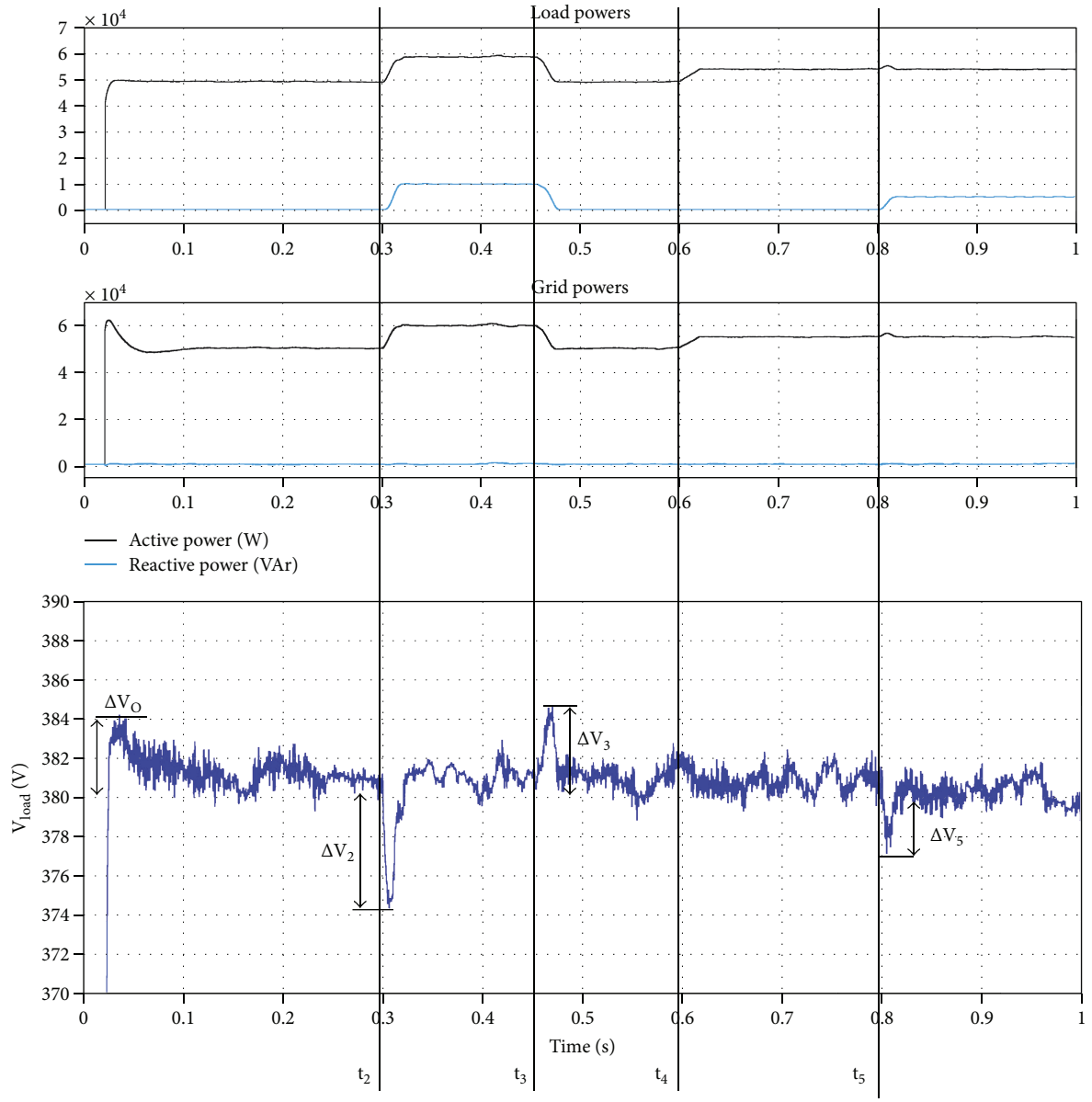

Figure 16: Reactive power compensation when the STATCOM device with a PI$^{\lambda}$-MPC hybrid controller is enabled and load voltage change.

4. Conclusion

In the study, the performance of the STATCOM device using a PI$^{\lambda}$-MPC hybrid controller has been investigated and compared with the version using a PI-type controller to eliminate the reactive power on loads fed by off-grid solar panels. The system was forced by constantly changing the ambient temperature and the solar irradiation level as well as the loads, and the efficiencies of the controllers were tried to be shown meanwhile.

In the system, V_{DC} voltage was controlled by PI$^{\lambda}$ and the switching signals in a 24 IGBTs 5-level STATCOM device were controlled by MPC. The most important reason for this is that PID-type controllers can be placed everywhere comfortably, while it is necessary to use detailed mathematical equations for designing MPCs. This makes MPCs difficult to design. However, the controllers with different PID types can be placed easily everywhere that errors are in. MPC controls the switching signals in the STATCOM device. It works more efficiently because it chose the right and the best one from the switching possibilities. V_{DC} voltage was controlled by PI$^{\lambda}$ that is able to adjust more precisely than PI. By combining these two controllers, a hybrid controller was created.

The comparison of STATCOM device results obtained from PI and PI$^{\lambda}$-MPC controllers shows that PI$^{\lambda}$ V_{DC} overshoot parameters are better than PI because PI$^{\lambda}$ overshoot is 213 V and PI overshoot is 230 V. Similarly, the reactive power overshoot value for a PI controller is 70 kVAr. But MPC has no overshoot. PI$^{\lambda}$ load voltage overshoot is 384 V; PI controller load voltage overshoot is 465 V.

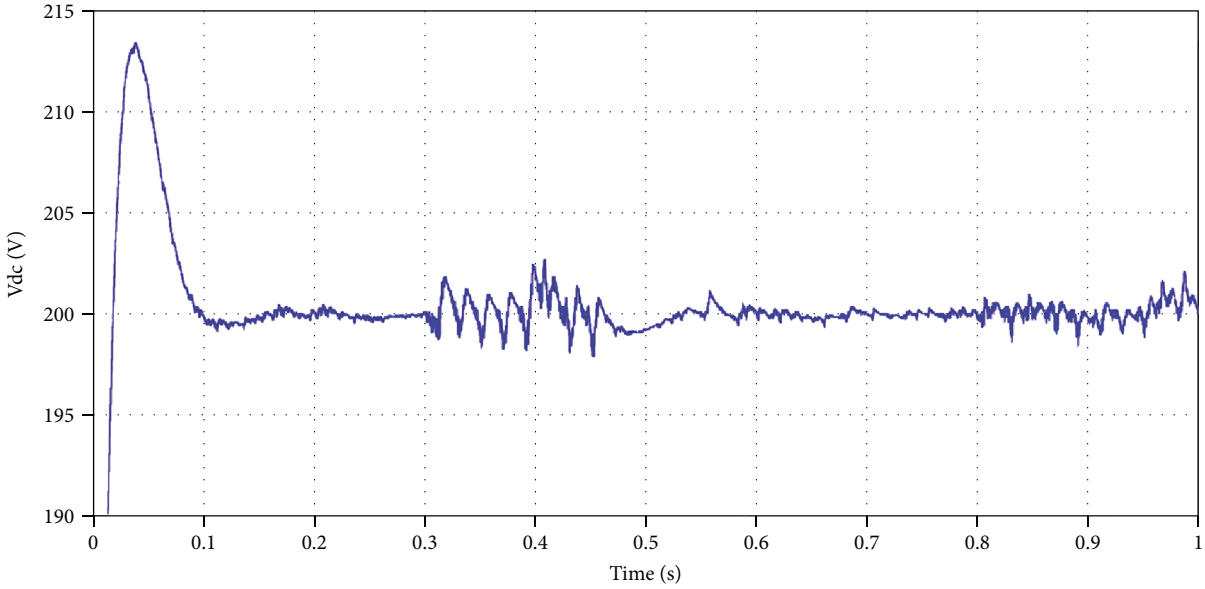

Figure 17: Capacitor voltage control in the STATCOM device with a PI$^{\lambda}$-MPC hybrid controller.

PI$^{\lambda}$ V_{DC} settling times are better than those of PI. The PI$^{\lambda}$ settling time is 0.1 ms, and the PI settling time is 0.3 ms for the steady state. The reactive power settling time is 0.02 ms for a PI controller and MPC is approximately 0 ms, and finally, the load voltage settling time is 0.05 ms for a PI controller and 0.02 ms for a PI$^{\lambda}$ controller.

If we compare steady state errors, PI$^{\lambda}$ and PI controllers are equal for the V_{DC} steady state error parameter and load voltage steady state error parameter. V_{DC} steady state error is 0 in both PI and PI$^{\lambda}$ controllers. The load voltage steady state error change range is ±6V in both PI and PI$^{\lambda}$ controllers. But reactive power steady state error is better than MPC. MPC steady state error is 50 VAr, and the PI controller value is 300 VAr.

The results of the FFT analysis show that the PI$^{\lambda}$-MPC controller is better than the PI controller. Total harmonic distortion of the PI$^{\lambda}$-MPC controller is 4.94% for voltage analysis and 4.17% for current analysis, and then PI controller FFT analysis for voltage is 5.05% and current is 4.18%.

As mentioned in the previous paragraph, the reactive power compensation performed very well and the error rates were very weak. The overshoot values of PI controllers were higher than those of PI$^{\lambda}$-MPC hybrid controllers. Also, the settling time values were shorter on the PI$^{\lambda}$-MPC hybrid controller. In general, the performance of the PI$^{\lambda}$-MPC hybrid controller is much better than those of PI controllers.

Conflicts of Interest

The author declares that they have no conflicts of interest.

References

[1] I. H. Altas and A. M. Sharaf, "A novel on-line MPP search algorithm for PV arrays," *IEEE Transactions on Energy Conversion*, vol. 11, no. 4, pp. 748–754, 1996.

[2] T. D. Lee and A. U. Ebong, "A review of thin film solar cell technologies and challenges," *Renewable and Sustainable Energy Reviews*, vol. 70, pp. 1286–1297, 2017.

[3] J. Praveen and V. VijayaRamaraju, "Materials for optimizing efficiencies of solar photovoltaic panels," *Materials Today: Proceedings*, vol. 4, no. 4, Part D, pp. 5233–5238, 2017.

[4] S. C. W. Krauter, *Solar Electric Power Generation*, Springer, New York, NY, USA, 2006.

[5] S. Sumathi, L. A. Kumar, and P. Surekha, *Solar PV and Wind Energy Conversion Systems*, Springer, Switzerland, 2015.

[6] V. Chamola, B. Krishnamachari, and B. Sikdar, "Green energy and delay aware downlink power control and user association for off-grid solar-powered base stations," *IEEE Systems and Journal*, vol. PP, no. 99, pp. 1–12, 2017.

[7] L. Luo, W. Gu, X.-P. Zhang et al., "Optimal siting and sizing of distributed generation in distribution systems with PV solar farm utilized as STATCOM (PV-STATCOM)," *Applied Energy*, vol. 210, pp. 1092–1100, 2018.

[8] P. R. Yelpale, H. T. J. Hod, and C. Charmole, "New control strategy for grid integrated PV solar farm to operate as STATCOM," in *2017 International Conference on Circuit, Power and Computing Technologies (ICCPCT)*, Kollam, India, April 2017.

[9] R. Sirjani and A. R. Jordegi, "Optimal Placement and Sizing of Distribution Static Compensator (D-STATCOM) in Electric Distribution Networks: A review," *Renewable and Sustainable Energy Reviews*, vol. 77, no. 4, pp. 688–694, 2017.

[10] H. Yonezawa, M. Tsukada, and J. J. Paserba, "Study of a STATCOM application for voltage stability evaluated by dynamic PV curves and time simulations," in *2000 IEEE Power Engineering Society Winter Meeting*, pp. 1471–1476, Singapore, Singapore, January 2000.

[11] S. Eshtehardiha, M. B. Poodeh, and M. R. Zare, "Improvement of STATCOM performance with multi variable control methods," in *IET-UK International Conference on Information and Communication Technology in Electrical Sciences (ICTES 2007)*, pp. 105–111, Tamil Nadu, India, December 2007.

[12] K. Rao and N. Patel, "Effectuation in SPWM technique for 3-Φ VSI using STM32F4 discovery board interfaced with MATLAB," in *2016 IEEE 7th Power India International Conference (PIICON)*, Bikaner, India, November 2016.

[13] F. L. Luo and H. Ye, *Advenced DC/AC Inverters*, CRC Press, USA, 2013.

[14] Z. Wu, C. Xu, and Y. Yang, "Adjustable PID control based on adaptive internal model and application in current shared control of multi inverters," *Journal of the Franklin Institute*, vol. 354, no. 7, pp. 2699–2711, 2017.

[15] A. Saygın and A. Kerem, "Fuzzy logic based control of a loaded asynchronous motor using a 6-switched 3-level inverter," in *2017 18th International Conference on Computational Problems of Electrical Engineering (CPEE)*, pp. 1–4, Kutna Hora, Czech Republic, September 2017.

[16] I. Rasoanarivo, K. Arab-Tehrani, and F. M. Sargos, "Fractional order PID and modulated hysteresis for high performance current control in multilevel inverters," in *2011 IEEE Industry Applications Society Annual Meeting (IAS)*, pp. 1–7, Orlando, FL, USA, October 2011.

[17] H. Soliman, I. Abdelsalam, H. Wang, and F. Blaabjerg, "Artificial neural network based DC-link capacitance estimation in a diode-bridge front-end inverter system," in *2017 IEEE 3rd International Future Energy Electronics Conference and ECCE Asia (IFEEC 2017 - ECCE Asia)*, pp. 196–201, Kaohsiung, Taiwan, June 2017.

[18] M. R. B. Fathima, P. M. J. Princy, and S. R. Prasath, "Mathematical modeling of SVPWM ınverter fed 3 phase induction motor vector control in MATLAB/Simulink environment," in *2017 International Conference on Circuit, Power and Computing Technologies (ICCPCT)*, pp. 1–8, Kollam, India, April 2017.

[19] J. Su and D. Sun, "Model predictive torque-vector control for four-switch three-phase inverter-fed PMSM with capacitor voltage offset suppression," in *Electrical Machines and Systems (ICEMS)*, pp. 1–5, Sydney, New South Wales, Australia, August 2017.

[20] S. Qian, Y. Ye, H. Wu, and Z. Zhuang, "Optimizing PWM switching sequence of inverters using an immune genetic algorithm," in *2016 8th International Conference on Intelligent Human-Machine Systems and Cybernetics (IHMSC)*, pp. 7–10, Hangzhou, China, August 2016.

[21] I. H. Altas and A. M. Sharaf, "A photovoltaic array simulation model for MATLAB-Simulink GUI environment," in *2007 International Conference on Clean Electrical Power*, pp. 341–345, Capri, Italy, May 2007.

[22] I. H. Altas and A. M. Sharaf, "A novel maximum power fuzzy logic controller for photovoltaic solar energy systems," *Renewable Energy*, vol. 33, no. 3, pp. 388–399, 2008.

[23] M. A. S. Masoum, H. Dehbonei, and E. F. Fuchs, "Theoretical and experimental analyses of photovoltaic systems with voltage and current-based maximum power-point tracking," *IEEE Transactions on Energy Conversion*, vol. 17, no. 4, pp. 514–522, 2002.

[24] B. Singh, K. Al-Haddad, R. Saha, and A. Chandra, "Static synchronous compensators (STATCOM): a review," *IET Power Electronics*, vol. 2, no. 4, pp. 297–324, 2009.

[25] N. G. Hingorani and L. Gyugti, *Understanding FACTS, Consepts and Technology of Flexible AC Transmission Systems*, IEEE Press, USA, 2000.

[26] K. Yanmaz, I. H. Altas, and O. O. Mengi, "Five level cascaded H-bridge D-STATCOM using a new fuzzy and PI controllers model for wind energy systems," *Advances in Electrical and Computer Engineering*, vol. 17, no. 4, pp. 49–58, 2017.

[27] P. Shah and S. Agashe, "Review of fractional PID controller," *Mechatronics*, vol. 38, pp. 29–41, 2016.

[28] I. Rasoanarivo and F. M. Sargos, "Multi-objective analysis for designing and controlling microgrids under multi-control with PID, MHCC and FOPID controllers," in *2013 IEEE Industry Applications Society Annual Meeting*, pp. 7–10, Lake Buena Vista, FL, USA, October 2013.

[29] A. Tepljakov, E. Petlenkov, and J. Belikov, "FOMCON: fractional-order modeling and control toolbox for MATLAB," in *2011 Proceedings of the 18th International Conference Mixed Design of Integrated Circuits and Systems (MIXDES)*, pp. 684–689, Gliwice, Poland, June 2011.

[30] S. Vazquez, J. Rodriguez, M. Rivera, L. G. Franquelo, and M. Norambuena, "Model predictive control for power converters and drives: advances and trends," *IEEE Transactions on Industrial Electronics*, vol. 64, no. 2, pp. 935–947, 2017.

[31] J. Rodriguez and P. Cortes, *Predictive Control of Power Converters and Electrical Drives*, Wiley-IEEE Press, United Kingdom, 2012.

[32] I. Rasoanarivo, P. Boos, and B. Davat, "Improvements of parallel active filter performances," in *EPE'97*, pp. 898–902, Trondheim, Norway, September 1997.